Time-Dependent Nanomechanics of Cartilage (Supporting Material)

Lin Han,[†] Eliot H. Frank,[‡] Jacqueline J. Greene,[†] Hsu-Yi Lee,[§] Han-Hwa Hung,[‡] Alan J Grodzinsky,[‡§¶‖] and Christine Ortiz[†]*

[†]Department of Materials Science and Engineering, [‡]Center for Biomedical Engineernig, [§]Department of Electrical Engineering and Computer Science, [¶]Department of Mechanical Engineering, and [‖]Department of Biological Engineering, Massachusetts Institute of Technology, Cambridge, Massachusetts

APPENDIX

A. Analysis of AFM-based indentation curves

For each AFM-based indentation experiment, the raw data outputs were the cantilever deflection (d_V, in volts) and z-piezo displacement (z, in nm). To calculate forces, F (nN), calibration of the cantilever deflection sensitivity, d_s (nm/V) was first performed via measurement of cantilever bending on a hard mica surface, and the spring constant k (nN/nm) was measured via thermal vibration (1). Force was then calculated as $F = d_V \times d_s \times k$. For each indentation curve, the z-piezo displacement z was adjusted by subtracting the cantilever deflection d (in nm, $d = d_V \times d_s$), $z' = z - d$. Force data F were slightly offset by subtracting a small value (e.g., 10^{-6} nN) from the measured minimum value to ensure positive definite values along the force curve.

To calculate the indentation depth D, the contact point between the probe tip and cartilage disk must be determined. In all the experiments of this study, no attractive or adhesive interactions were observed between the tip and cartilage. Hence, we adapted a previously reported method (2) to determine the effective tip-sample contact point in the absence of adhesion. In order to remove the spurious portion of the curve that contains no detectable force signals, two positions were searched via the cubic spline fit on the loading curve of log F versus z' in the direction of tip moving towards the sample (2). The first position, z_1, was taken as the last data point at which the first derivative of the fit is negative and second derivative is positive ($d\log F/dz' < 0$ and $d^2\log F/dz'^2 > 0$). The second position, z_2, was taken as the last data point prior to z_1 where $d\log F/dz' > 0$ and $d^2\log F/dz'^2 < 0$, or the first data point along the curve if no data point was detected via the former scenario. The noise level of the force data, n_F, was taken as the 95th percentile of log$F$ for the data between z_1 and z_2. The zero force data point, z_0, was determined as the last data point along the curve where the force signal was below the noise level, $\log F < n_F$. After the removal of the spurious data ($z' < z_0$), the remaining portion of the F versus z' curve was converted to force (F) versus indentation depth (D) using $D = z' - z_0$.

For indentation on microtomed cartilage disks, there were sometimes small long range repulsion forces between the cartilage and the neutral probe tip prior to tip-sample contact, possibly due to electrostatic repulsion from the negatively charged aggrecan (3) and/or the presence of microtomed collagen fibrils on the cartilage disk surface. The effective tip-cartilage disk contact point, (D_0, F_0), was determined via the Golden Section search method along the F versus D curve. This effective contact point was taken as the point corresponding to the minimal weighted root mean square error from two least square linear regressions: the linear fit in the noncontant region (LSLR of F versus D, $D < D_0$) and the polynomial fit in the contact region (LSLR of $(F - F_0)$ versus $(D - D_0)^m$, m = 1.5 for spherical tip and m = 2 for pyramidal tip), with errors in the noncontact region weighted half (2). The F versus D curve, which represents indentation of the cartilage disk, was thereby corrected by trimming the noncontact region and offsetting the remaining F-D data by (D_0, F_0).

As negligible irreversible plastic deformation was observed upon repeated indentation at the same location (Fig. 1b), we utilized loading curves to estimate the effective indentation modulus E_{ind} via the analytical models Eqs. (1) and (2) assuming linear, isotropic, and elastic material behavior. The validity of the analytical model for the geometry (e.g., Hertz model for spherical indentation) was tested by comparing the modulus calculated via Hertz model to that calculated via finite element modeling, and < 1% difference was found between these two methods. In the tested indentation depth range, fitting different portions of the loading curve yielded similar E_{ind}, suggesting that the cartilage behaved linearly within the tested range (4). Previous AFM-based nanoindentation studies of bovine knee cartilage utilizing the Hertz model and the loading portion of the curve have reported similar E_{ind} values (5,6). Differences in the magnitude of the reported indentation moduli in other studies were possibly due to different cartilage species (7,8), different experimental parameters (e.g., applied force, indentation rate) and data analysis methods (e.g., the Oliver-Pharr method (9) on the unloading curve) (10-12), and/or different magnitudes of deformation (e.g., deformations up to hundreds of μm via an instrumented nanoindenter) (13-17).

B. Calibration and analysis of dynamic oscillatory indentation data

To correct for any systematic errors in the AFM-based dynamic indentation measurements, calibration was first

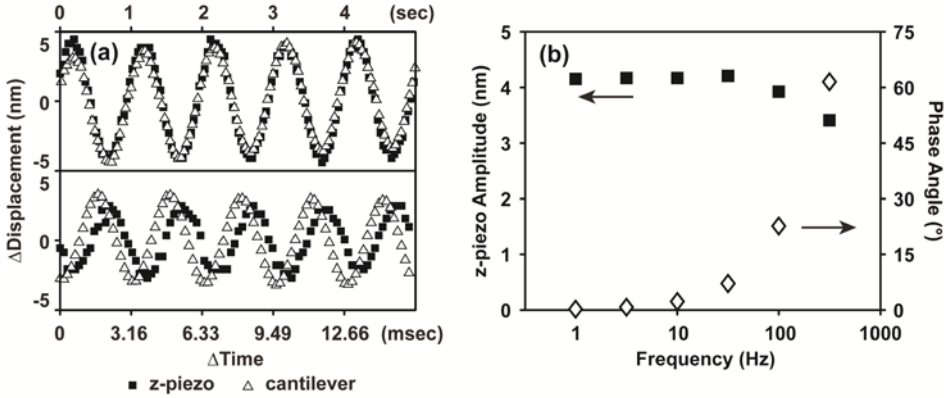

FIGURE A1 (a) Sampling of 5 cycles of z-piezo displacement (solid squares) and simultaneous cantilever deflection data (open triangles) during the dynamic oscillation of z-piezo using a spherical probe tip (R ~ 2.5 μm) on a hard mica surface in MilliQ water at 1 Hz, ~ 4 nm amplitude and 316 Hz, ~ 3 nm amplitude. One of every 40 data points were plotted for the 1 Hz (upper panel) and every other data point were plotted for the 316 Hz (lower panel). (b) Estimated z-piezo displacement amplitude (solid squares) and phase angle (deflection – z-piezo displacement, open diamonds) as a function of input frequency f at ~ 4 nm z-piezo displacement amplitudes. All data were obtained on a mica surface in MilliQ water ($n \geq 6$ different locations, mean, SEM was smaller than the size of data symbols).

carried out on a hard mica surface at the same z-piezo displacement frequencies and amplitudes as for the cartilage disks. At each measurement frequency and amplitude, five cycles of the sinusoidal dynamic z-piezo displacement, $\tilde{z}$, and cantilever deflection, $\tilde{d}$, data were randomly chosen in the steady state, which was achieved by 15 seconds after start of the oscillation (Fig. A1a). The z-piezo and deflection data were offset by their means, and subjected to least squares nonlinear regression,

$$\tilde{d}_0 = \tilde{d}_{a0} \sin(2\pi f t + \psi_0), \tag{A1}$$

$$\tilde{z}_0 = \tilde{z}_{a0} \sin(2\pi f t + \phi_0), \tag{A2}$$

where $\tilde{d}_0$, $\tilde{z}_0$ and t are the measured dynamic cantilever deflection (nm), z-piezo displacement (nm) and time (sec), f the frequency, while amplitudes $\tilde{d}_{a0}$, $\tilde{z}_{a0}$, and phase angles ψ_0, ϕ_0 are the initial best fit values of those parameters (the subscript "0" denotes the fit from the calibration sample). These initial guesses were set at the maximum of $\tilde{d}_0$ for $\tilde{d}_{a0}$, maximum of $\tilde{z}_0$ for $\tilde{z}_{a0}$, and for ψ_0, ϕ_0, the arcsine value of the first deflection/z-displacement data point normalized by the maximum. If the fit resulted in $R^2 > 0.8$, the outputs of the fit ($\hat{\tilde{z}}_{a0}, \hat{\tilde{d}}_{a0}, \hat{\phi}_0, \hat{\psi}_0$, where "^" denotes the fit output) were accepted as the values for that one sample. To eliminate possible errors from external noise and random data sampling, for each amplitude and frequency, this procedure was repeated until 50 samples were collected. The final data output values were calculated as the average value from the 50 pairs of regression outputs.

Given the essentially infinite stiffness of mica compared to that of the AFM cantilever, the amplitudes of $\tilde{z}_0$ and $\tilde{d}_0$ were observed to be independent of frequency for $f \leq 100$ Hz, and measurements showed that $\hat{\tilde{z}}_{a0} = \hat{\tilde{d}}_{a0}$ (Fig. A1a, upper panel). However, for $f > 100$ Hz, $\hat{\tilde{z}}_{a0} < \hat{\tilde{d}}_{a0}$ was observed, due to the attenuation of the high frequency z-piezo displacement signal by the low pass filter implemented as part of the z-sensor (18) (Fig. A1a, lower panel). Hence, for f = 316 Hz, the values of $\hat{\tilde{d}}_{a0}$ were taken to be the z-piezo displacement amplitudes (Fig. A1b). Changes in the phase angle between $\tilde{z}_0$ and $\tilde{d}_0$ $(\hat{\psi}_0 - \hat{\phi}_0)$ were observed at higher frequencies that were also associated with the low-pass filters and displacement sensors (18) and, to a much lesser extent, the hydrodynamic drag effect (19). Such changes in the phase angle from these calibration measurements were subtracted from experimental (cartilage) data, as described below.

For each dynamic oscillatory curve taken on the cartilage disks, the same sampling procedure, as for the calibration data, was repeated, and least-square nonlinear regression was performed on z-piezo and deflection data, $\tilde{z}$ and $\tilde{d}$,

$$\tilde{d} = \tilde{d}_a \sin(2\pi f t + \psi), \tag{A3}$$

$$\tilde{z} = \tilde{z}_a \sin(2\pi f t + \phi), \tag{A4}$$

where t, $\tilde{d}$ and $\tilde{z}$ are the experiment outputs, and the initial values for $\tilde{d}_a$, $\tilde{z}_a$, ψ and ϕ were estimated in the same fashion as for the calibration data. Only fits resulting

in $R^2 > 0.9$ for both cantilever deflection and z-piezo data were accepted. The corresponding complex numbers representing the amplitudes and phase of z-piezo and cantilever deflection were calculated after correction in amplitude ($\hat{\tilde{z}}_a = \hat{\tilde{d}}_{a0}$ for f = 316 Hz) and phase angle via calibration:

$$\tilde{\mathbf{d}} = \hat{\tilde{d}}_a\left[\cos\left(\hat{\psi} + \hat{\phi}_0 - \hat{\psi}_0\right) + i\sin\left(\hat{\psi} + \hat{\phi}_0 - \hat{\psi}_0\right)\right], \quad \text{(A5)}$$

$$\tilde{\mathbf{z}} = \hat{\tilde{z}}_a\left(\cos\hat{\phi} + i\sin\hat{\phi}\right). \quad \text{(A6)}$$

The complex amplitudes (magnitude and phase) of dynamic indentation depth, $\tilde{\mathbf{D}}$, and force, $\tilde{\tilde{\mathbf{F}}}$, were calculated as $\tilde{\mathbf{D}} = \tilde{\mathbf{z}} - \tilde{\mathbf{d}}$, and $\tilde{\tilde{\mathbf{F}}} = \tilde{\mathbf{d}} \times k$, respectively. For each dynamic oscillation curve, the phase $\delta(f)$ between $\tilde{\mathbf{D}}$ to $\tilde{\tilde{\mathbf{F}}}$ and the magnitude of complex dynamic modulus $|E^*|$ were calculated as the average of 100 sampling results using the analytical models, Eqs. (5) and (6), as shown in Figs. 3 – 6.

REFERENCES

1. Hutter, J. L. and J. Bechhoefer. 1993. Calibration of atomic-force microscope tips. *Rev. Sci. Instrum.* 64:1868-1873.
2. Lin, D. C., E. K. Dimitriadis and F. Horkay. 2007. Robust strategies for automated AFM force curve analysis - I. Non-adhesive indentation of soft, inhomogeneous materials. *J. Biomech. Eng.* 129:430-440.
3. Dean, D., L. Han, …, C. Ortiz. 2006. Compressive nanomechanics of opposing aggrecan macromolecules. *J. Biomech.* 39:2555-2565.
4. Mahaffy, R. E., C. K. Shih, …, J. Kas. 2000. Scanning probe-based frequency-dependent microrheology of polymer gels and biological cells. *Phys. Rev. Lett.* 85:880-883.
5. Park, S., K. D. Costa, …, K.-S. Hong. 2009. Mechanical properties of bovine articular cartilage under microscale indentation loading from atomic force microscopy. *Proc. Inst. Mech. Eng. [H].* 223:339-347.
6. Park, S., K. D. Costa and G. A. Ateshian. 2004. Microscale frictional response of bovine articular cartilage from atomic force microscopy. *J. Biomech.* 37:1679-1687.
7. Hu, K., P. Radhakrishnan, …, J. J. Mao. 2001. Regional structural and viscoelastic properties of fibrocartilage upon dynamic nanoindentation of the articular condyle. *J. Struct. Biol.* 136:46-52.
8. Radhakrishnan, P., N. T. Lewis and J. J. Mao. 2004. Zone-specific micromechanical properties of the extracellular matrices of growth plate cartilage. *Ann. Biomed. Eng.* 32:284-291.
9. Oliver, W. C. and G. M. Pharr. 1992. An improved technique for determining hardness and elastic modulus using load and displacement sensing indentation experiments. *J. Mater. Res.* 7:1564-1583.
10. Stolz, M., R. Raiteri, …, U. Aebi. 2004. Dynamic elastic modulus of porcine articular cartilage determined at two different levels of tissue organization by indentation-type atomic force microscopy. *Biophys. J.* 86:3269-3283.
11. Stolz, M., R. Gottardi, …, U. Aebi. 2009. Early detection of aging cartilage and osteoarthritis in mice and patient samples using atomic force microscopy. *Nat. Nanotechnol.* 4:186-192.
12. Loparic, M., D. Wirz, …, M. Stolz. 2010. Micro- and nanomechanical analysis of articular cartilage by indentation-type atomic force microscopy: validation with a gel-microfiber composite. *Biophys. J.* 98:2731-2740.
13. Franke, O., K. Durst, …, K. Gelse. 2007. Mechanical properties of hyaline and repair cartilage studied by nanoindentation. *Acta Biomaterialia.* 3:873-881.
14. Li, C., L. Pruitt and K. B. King. 2006. Nanoindentation differentiates tissue-scale functional properties of native articular cartilage. *J. Biomed. Mater. Res. A.* 78A:729-738.
15. Ebenstein, D. M., A. Kuo, …, L. Pruitt. 2004. A nanoindentation technique for functional evaluation of cartilage repair tissue. *J. Mater. Res.* 19:273-281.
16. Gupta, S., J. Lin, …, L. Pruitt. 2009. A fiber reinforced poroelastic model of nanoindentation of porcine costal cartilage: a combined experimental and finite element approach. *J. Mech. Behav. Biomed. Mater.* 2:326-338.
17. Miller, G. J. and E. F. Morgan. 2010. Use of microindentation to characterize the mechanical properties of articular cartilage: comparison of biphasic material properties across length scales. *Osteoarthritis Cartilage.* 18:1051-1057.
18. Asif, S. A. S., K. J. Wahl, …, O. L. Warren. 2001. Quantitative imaging of nanoscale mechanical properties using hybrid nanoindentation and force modulation. *J. Appl. Phys.* 90:1192-1200.
19. Alcaraz, J., L. Buscemi, …, D. Navajas. 2002. Correction of microrheological measurements of soft samtples with atomic force microscopy for the hydrodynamic drag on the cantilever. *Langmuir.* 18:716-721.